Research in Astronomy and Astrophysics, 25:105004 (8pp), 2025 October
https://doi.org/10.1088/1674-4527/adf1ed
CSTR: 32081.14.RAA.adf1ed
© 2025. National Astronomical Observatories, CAS and IOP Publishing Ltd. All rights, including for text and data mining, AI training, and similar technologies, are reserved. Printed in China.

Statistical Characteristics of Solar Cycle Distribution of N–S Asymmetry for the Source Locations of Super Geomagnetic Storms (Dst $\leqslant -250$ nT) During 1932–2018

Qi Li[1] and Gui-Ming Le[2,3]
[1] Institute of Geophysics, China Earthquake Administration, Beijing 100081, China
[2] Key Laboratory of Space Weather, National Satellite Meteorological Center (National Center for Space Weather), China Meteorological Administration, Beijing 100081, China; Legm@cma.gov.cn
[3] Innovation Center for FengYun Meteorological Satellite (FYSIC), Beijing 100081, China
Received 2025 May 3; revised 2025 June 11; accepted 2025 June 13; published 2025 August 15

Abstract

Partitioning the solar cycle into ascending and descending phases, we examine the solar cycle distribution of the north–south (N–S) asymmetry in the source locations of super geomagnetic storms (SGSs; Dst $\leqslant -250$ nT) during 1932–2018. We found that during the ascending phases, SGS source locations were predominantly in the northern hemisphere (NH), exhibiting significant N–S asymmetry. For the SGSs in the descending phases, source locations of the SGSs dominated in the NH and N–S asymmetry was only significant in the western hemisphere. For the period from 1932 to 2018, the source locations of SGSs were predominantly in the NH, and the N–S asymmetry was significant. The cumulative numbers of SGSs originating from the two hemispheres were strongly anticorrelated during the ascending phases, descending phases, and the entire period from 1932 to 2018. For the source locations of SGSs with different intensities, significant N–S asymmetries were observed in the source location distribution. Specifically, for all SGSs, SGSs with -400 nT $<$ Dst $\leqslant -300$ nT, and SGSs with Dst $\leqslant -300$ nT, the NH exhibited a higher number of events compared to the southern hemisphere (SH), indicating a dominance of SGSs in the NH. From the perspective of the evolution of N–S asymmetry with the solar cycle, the source locations of the SGSs always dominated in the NH during the ascending phases. However, during solar cycles 17–19 and 21, the source locations of the SGSs dominated in the NH, while during solar cycles 20, 22, and 23 the source locations of the SGSs dominated in the SH. From the perspective of N–S asymmetry for Solar Cycles 17–23, solar activity across the two hemispheres is largely balanced. However, the solar activities manifested by CMEs that can trigger SGSs during Solar Cycles 17–23 were predominantly in the NH. Therefore, factors beyond solar activity, such as the propagation of the CMEs from the Sun to the Earth, likely contribute to the observed N–S asymmetric distribution of the source locations of SGSs.

Key words: (Sun:) sunspots – Sun: coronal mass ejections (CMEs) – (Sun:) solar-terrestrial relations

1. Introduction

A geomagnetic storm is a major disturbance of Earth's magnetosphere. The current systems in the magnetosphere are very complex during the period of a geomagnetic storm (e.g., Maltsev 2004; Dubyagin et al. 2014; Ganushkina et al. 2015). The ring current exerts a substantial influence on the Dst index. The intensity of the ring current is inversely correlated with the Dst index: the stronger the ring current, the more negative the Dst index becomes. Consequently, the Dst index serves as a proxy for ring current intensity. This is precisely why the Dst index is utilized to characterize the intensity of geomagnetic storms. Ring current particles lead to a series of space weather effects (e.g., Lakhina et al. 2012; Ganushkina et al. 2017). A geomagnetic storm with Dst $\leqslant -250$ nT is defined as a super geomagnetic storm (SGS). Zhao et al. (2023) studied the average rate of change of the ring current during the main phase of SGSs. Being relatively rare, SGSs are extreme space weather phenomena that can only be caused by coronal mass ejections (CMEs) (e.g., Gosling et al. 1991; Huttunen et al. 2002b; Zhang et al. 2007; Richardson & Cane 2012; Yermolaev et al. 2013). CMEs are large expulsions of plasma and magnetic field from active regions (ARs). It is found that 50% of SGSs are produced by super active regions (Le et al. 2021a). Cliver et al. (2022) found that a considerable part of the CMEs producing the geomagnetic storms with Dst $\leqslant -300$ nT originate from the ARs with area $\leqslant$1000 millionths of a solar hemisphere.

Many articles have been devoted to the source locations of single or some SGSs (e.g., Garcia & Dryer 1987; Cliver & Crooker 1993; Huttunen et al. 2002a; Yermolaev et al. 2008; Gopalswamy et al. 2005a, 2005b, 2022; Zhang et al. 2007; Lefèvre et al. 2016; Meng et al. 2019; Cliver et al. 2022). It was found that fast halo CMEs with source locations close to

Table 1
Numbers of SGSs in the NH and the SH During Different Phases of Solar Cycles

Period	Number of SGSs	Dominance	$P(\geqslant d)$	p-value of χ^2 Test
Ascending phases	$N_n = 14$, $N_s = 4$	NH	$1.544 \times 10^{-2} < 5\%$	$0.0027 < 0.05$
Descending phases	$N_n = 21$, $N_s = 12$	NH	$8.138 \times 10^{-2} > 5\%$	$0.0489 < 0.05$
1932–2018	$N_{250n} = 12$, $N_{250s} = 9$	NH	$3.320 \times 10^{-1} > 10\%$	$0.5371 > 0.05$
	$N_{300n} = 16$, $N_{300s} = 5$	NH	$1.330 \times 10^{-2} < 5\%$	$0.0020 < 0.05$
	$N_{400n} = 7$, $N_{400s} = 2$	NH	$8.980 \times 10^{-2} > 5\%$	$0.0593 > 0.05$
	$N_{\leqslant 300n} = 23$, $N_{\leqslant 300s} = 7$	NH	$2.611 \times 10^{-3} < 5\%$	$0.0001 < 0.05$
	$N_{\leqslant 250n} = 35$, $N_{\leqslant 250s} = 16$	NH	$5.487 \times 10^{-3} < 5\%$	$0.0004 < 0.05$

the solar disk center are favorable candidates for strong geomagnetic storms (Venkatakrishnan & Ravindra 2003; Srivastava 2005). Meng et al. (2019) found that the source locations of the most flares associated with the CMEs that produced SGSs are confined within 30° heliolongitude. As the Dst index was reconstructed back to 1932 (Karinen & Mursula 2005), Le et al. (2021a) studied the source locations of the great geomagnetic storms (GGSs, Dst $\leqslant -200$ nT) and found that 90% of the source locations of the GGSs were confined in the heliolongitudinal area of [E45, W45], and the source locations of the geomagnetic storms with Dst $\leqslant -400$ nT are confined in the heliolongitude area of [E22, W14]. These results indicate that only the CMEs with source locations around the solar disk center can produce very strong geomagnetic storms. Statistical results show that much more GGSs appear in the descending phases than in the ascending phases (Le et al. 2021b). All CMEs that triggered SGSs are halo CMEs. Zhang et al. (2024) investigated the north–south (N–S) asymmetry in the source locations of halo CMEs. However, the statistical properties of the N–S asymmetry of the source locations of the SGSs during the ascending and descending phases of solar cycles (SCs) have not been investigated. In addition, the statistical properties of the N–S asymmetry of the source locations of the SGSs with different intensities have not been reported. The number of SGSs during 1957–2018 is 39 (Meng et al. 2019), while the number of SGSs during 1932–2018 is 54 (Le et al. 2021b), indicating that the period from 1932 to 2018 has many more SGSs than the period from 1957 to 2018. The distributions of various extreme space weather phenomena across SCs have been extensively studied (e.g., Kilpua et al. 2015; Hajra et al. 2016; Lefèvre et al. 2016; Vennerstrom et al. 2016; Meng et al. 2019; Chapman et al. 2020; Le & Liu 2020; Le et al. 2021b, 2021c, 2021d; Owens et al. 2021; Zhao et al. 2022; Chapman & Dudok de Wit 2024). Some studies analyzed solar —activity phenomena across the four canonical phases of the SC—ascending, maximum, descending, and minimum (e.g., Kilpua et al. 2015; Meng et al. 2019; Li & Le 2025). If the cycle is instead divided simply into ascending and descending intervals, what are the statistical characteristics of the N-S asymmetry of SGS source locations from 1932 to 2018, and how does this asymmetry vary with storm intensity over the same period? The motivation of this study is to answer these questions. The remainder of this paper is organized as follows. Section 2 provides a comprehensive list of the source locations of the SGSs from 1932 to 2018. In Section 3, we present a detailed statistical analysis of the N–S asymmetries in the source locations of the SGSs across different phases of the SC. Section 4 is dedicated to a thorough discussion of the results. Finally, Section 5 concludes the paper with a summary and conclusions.

2. The Source Locations of the SGSs During 1932–2018

The Dcx and the Dxt indices, which can be treated as the Dst index, have been reconstructed back to 1932 and widely used (e.g., Yakovchouk et al. 2012; Lefèvre et al. 2016; Vennerstrom et al. 2016; Pick & Korte 2017; Love 2021; Takalo 2021). The Dxt index is closer to the Dst index (Riley 2018; Takalo 2021), which is used as the Dst index during 1932–1956. Smoothed monthly mean sunspot numbers (SMMSNs) are usually used to determine the progress of a SC. The largest SMMSNs during a SC are termed the amplitude of the SC. In this study, the period from the first month of a SC to the month when SMMSNs reach their largest value is defined as the ascending phase, while the period from one month after the largest SMMSNs to the last month of a SC is defined as the descending phase of the SC. An SGS may be associated with two or more CMEs (e.g., Wang et al. 2003; Zhang et al. 2007). Of the multiple CMEs associated with an SGS, only the CME that makes crucial contribution in producing the SGS is treated as the source location of the SGS. The source locations of the SGSs that occurred during 1932–2018 by SC are listed in the Table A1 in the Appendix. The source locations for the SGSs (Dst $\leqslant -300$ nT) were directly copied from the article Cliver et al. (2022). The information for each SC, the amplitude of the SC, the time information including year, month and day, source location and the reference for each SGS is given in Table 1. SMMSNs obtained from the website http://sidc.oma.be are used to describe the progress of a SC.

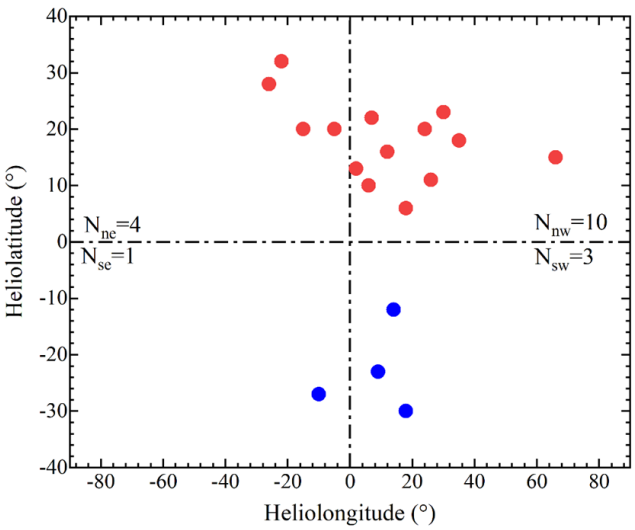


Figure 1. The source locations of the SGSs that occurred during the ascending phases from 1932 to 2018. Red solid circles represent SGSs originating in the NH, while blue solid circles indicate SGSs originating in the SH of the Sun.

3. N–S Asymmetric Distribution of the Source Locations of the SGSs

3.1. N–S Asymmetric Distribution of the Source Locations of the SGSs During Ascending Phases

To investigate the statistical properties of the N–S asymmetric distribution, we define the heliolatitude in the northern hemisphere (NH) as positive, while that in the southern hemisphere (SH) is defined as negative. For the convenience of description, we use N_{nw}, N_{ne}, N_{se} and N_{sw} to indicate the number of SGSs with source locations in the northwest, northeast, southeast, and southwest quadrants of the solar disk, respectively. The source locations of all the SGSs that appeared in the ascending phases are shown in Figure 1. As shown in Figure 1, N_{nw}, N_{ne}, N_{se} and N_{sw} are 10, 4, 1, and 3, respectively. The total number of source locations of SGSs in the northern and southern hemispheres are 14 and 4, respectively, indicating that the source locations of SGSs dominated in the NH for both the eastern and western hemispheres during the ascending phases.

3.2. N–S Asymmetric Distribution of the Source Locations of the SGSs During Descending Phases

The source locations of all the SGSs that appeared in the descending phases during 1932–2018 are shown in Figure 2. As shown in Figure 2, N_{nw}, N_{ne}, N_{se} and N_{sw} are 10, 11, 10, and 2, respectively. The numbers of the SGSs with source locations in the northern and southern hemispheres are 22 and 11, respectively, indicating that the source locations of the SGSs dominated in the NH. It is evident that the N–S symmetry is significant in the western hemisphere, and only the east–west (E–W) asymmetry is significant in the SH.

3.3. N–S Asymmetric Distribution of the Source Locations of SGSs with Different Intensity

We define N_{250n} and N_{250s} to represent the number of SGSs ($-300\,\mathrm{nT} < \mathrm{Dst} \leqslant -250\,\mathrm{nT}$) in the NH and SH, respectively. Similarly, N_{300n} and N_{300s} indicate the number of SGSs ($-400\,\mathrm{nT} < \mathrm{Dst} \leqslant -300\,\mathrm{nT}$) in the NH and SH, respectively. The variables N_{400n} and N_{400s} represent the number of SGSs ($\mathrm{Dst} \leqslant -400\,\mathrm{nT}$) in the NH and SH, respectively. Additionally, $N_{\leqslant 300n}$ and $N_{\leqslant 300s}$ indicate the number of SGSs ($\mathrm{Dst} \leqslant -300\,\mathrm{nT}$) in the NH and SH, respectively. Finally, we use $N_{\leqslant 250n}$ and $N_{\leqslant 250s}$ to represent the total number of SGSs with $\mathrm{Dst} \leqslant -250\,\mathrm{nT}$ originating from the northern and southern hemispheres, respectively, during the period from 1932 to 2018.

Figure 3 illustrates the N–S asymmetry in the source locations of all SGSs with different intensities during 1932–2018. The black solid circles highlight the minimal difference in the number of SGSs ($-300\,\mathrm{nT} < \mathrm{Dst} \leqslant -250\,\mathrm{nT}$). However, the NH exhibits a significantly higher number of SGSs (represented by red and blue solid circles) compared to the SH.

3.4. Statistical Test for N–S Asymmetry of the SGSs During Different Phases of Solar Cycles

The binomial formula (Larson 1982) is used to compute the probability of obtaining any particular distribution of n objects into two classes. Hence, it is widely used to check whether the N–S asymmetry is significant (e.g., Li & Gu 2000; Li et al. 2001; Joshi & Joshi 2004; Carbonell et al. 2007). In this study, these two classes correspond to the numbers of the SGSs in the northern and southern hemispheres. The binomial formula is given by

$$p(k) = \frac{n!}{(n-k)!k!}\left(\frac{1}{2}\right)^n. \quad (1)$$

The probability of obtaining more than d objects in class 1 is

$$P(\geqslant d) = \sum_{k=d}^{n} p(k). \quad (2)$$

If $P(\geqslant d) < 5\%$, then N–S asymmetry is significant. If $5\% < P(\geqslant d) < 10\%$, then N–S asymmetry is marginally significant. $P(\geqslant d) > 10\%$ implies that the N–S asymmetry is statistically insignificant. $P(\geqslant d)$ values for different periods were derived and listed in Table 1.

A χ^2 test for the numbers of the SGSs in the NH and the SH for different periods was made and the derived p-values of the χ^2 test are listed in the last column of Table 1. We found that the p-value of the χ^2 test is always lower than 0.05 when N–S asymmetry is significant, indicating that the number of the SGSs in NH has a strong anticorrelation with the number of the SGSs in SH. The p-value of the χ^2 test is always larger than 0.05 when N–S asymmetry is not significant, indicating that the number of SGSs in NH has no relation with the number of the SGSs in SH.

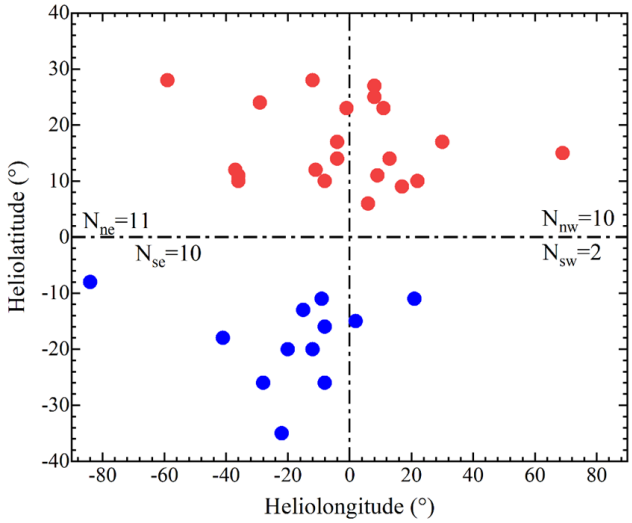


Figure 2. Source locations of the SGSs that appeared in the descending phases during 1932–2018. The red and blue solid circles indicate the SGSs with source locations in the northern and SH, respectively.

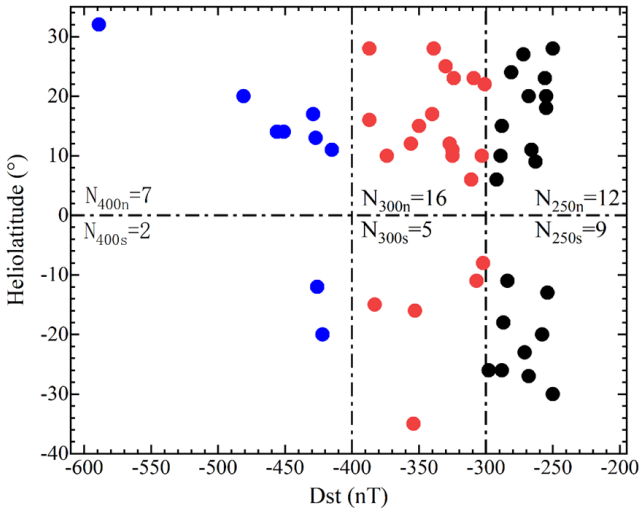


Figure 3. The source locations of all the SGSs during 1932–2018. The blue, red and black solid circles signify the geomagnetic storms with Dst $\leqslant -400$ nT, -400 nT $<$ Dst $\leqslant -300$ nT and -300 nT $<$ Dst $\leqslant -250$ nT, respectively.

4. Discussion

As indicated in the last column of Table 1, in the vast majority of cases, a strong anticorrelation is observed between the number of SGSs in the NH and the SH, suggesting a predominant distribution pattern in the source locations of the SGSs. However, in a few instances, no significant inverse correlation was found between the number of SGSs originating in the NH and SH.

Figures 1 and 2 demonstrate that the source locations of the SGSs were primarily in the NH during both the ascending and descending phases. Figure 3 reveals that the N–S asymmetry in

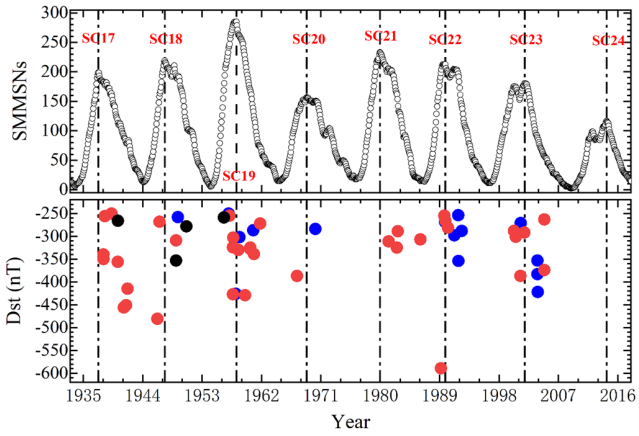


Figure 4. The evolution of the source locations of the SGSs with SC. Red and blue solid circles indicate the source locations of the SGSs in the northern and southern hemispheres, respectively. The black solid circles indicate the SGSs with source locations unknown.

the source locations of the SGSs from 1932 to 2018 is mainly due to the N–S asymmetry of the SGSs with Dst $\leqslant -300$ nT. For the cumulative number of SGSs during 1932–2018, there were 35 SGSs originating from the NH and 16 from the SH. This indicates that the source locations of SGSs during this period were predominantly in the NH. However, the distribution of the source locations of the SGSs shown in Figures 1–3 does not capture the evolution of the N–S asymmetry over the SC. As indicated in Table 1, the evolution of the source locations of the SGSs with respect to the SC is depicted in Figure 4. From Figure 4, it is evident that during the ascending phases, the source locations of the SGSs consistently dominated in the NH. During the descending phases, the source locations of the SGSs were predominantly in the NH for Solar Cycles 17–19 and 21, while they were predominantly in the SH during Solar Cycles 20, 22, and 23.

N–S asymmetry of solar activities is a phenomenon that has been observed and documented in various studies (e.g., Carbonell et al. 1993; Verma 1993; Ataç & Özgüç 1996; Joshi & Joshi 2004; Knaack et al. 2004; Temmer et al. 2006; Badalyan & Obridko 2011; Deng et al. 2017; Schüssler & Cameron 2018; Veronig et al. 2021; Zhang et al. 2022, 2024). Figures 1 and 2 illustrate the N–S asymmetries in the cumulative numbers of SGSs originating from the northern and southern hemispheres. Is the N–S asymmetry of solar activity, as indicated by the cumulative numbers of SGSs originating from the northern and southern hemispheres during both ascending and descending phases of SCs, consistent with the N–S asymmetry of cumulative sunspot numbers? To address this question, we first need to examine the N–S asymmetry in solar activity, as indicated by the cumulative sunspot numbers, during the ascending and descending phases of Solar Cycles 17–24. Based on the monthly mean sunspot numbers from 1874 to 2020 created by Veronig et al. (2021), which are available at the website https://cdsarc.cds.

Table 2
Cumulative Numbers of Sunspots and SGSs in the NH and SH During the Ascending and Descending Phases of SCs 17–24

SC	Ascending Phase							Descending Phase						
	N_{NASN}[a]	N_{SASN}[b]	DH_{ASN}[c]	DH_{ASGS}[d]	N_{NASGS}[e]	N_{SASGS}[f]	Unk[g]	N_{NDSN}[h]	N_{SDSN}[i]	DH_{DSN}[j]	DH_{DSGS}[k]	N_{NDSGS}[l]	N_{SDSGS}[m]	Unk
17	1578	18781	SH	null[n]	0	0	0	4455	4100	NH	NH	8	0	1
18	1557	2174	SH	NH	2	0	0	5102	4455	NH	Unk	1	1	1
19	3644	3491	NH	NH	4	2	1	5885	3254	NH	NH	6	2	0
20	2878	1463	NH	NH	1	0	0	3838	3759	NH	SH	0	1	0
21	2742	2144	NH	null	0	0	0	4146	5002	SH	NH	3	1	0
22	2047	1981	NH	NH	3	1	0	3819	4820	SH	SH	1	4	0
23	3700	3314	NH	NH	4	1	0	2013	3182	SH	SH	2	3	0
24	2040	1927	NH	null	0	0	0	1368	1196	NH	null	0	0	0

Notes.
[a] N_{NASN}: cumulative sunspot number in NH during ascending phase.
[b] N_{SASN}: cumulative sunspot number in SH during ascending phase.
[c] DH_{ASN}: dominant hemisphere of the cumulative sunspot number during ascending phase.
[d] DH_{ASGS}: dominant hemisphere of the cumulative number of SGSs during ascending phase.
[e] N_{NASGS}: cumulative number of SGSs in NH during ascending phase.
[f] N_{SASGS}: cumulative number of SGSs in SH during ascending phase.
[g] U_{nk}: the number of source locations of SGSs is unknown.
[h] N_{NDSN}: cumulative sunspot number in NH during descending phase.
[i] N_{SDSN}: cumulative sunspot number in SH during descending phase.
[j] DH_{DSN}: dominant hemisphere of the cumulative sunspot number during descending phase.
[k] DH_{DSGS}: dominant hemisphere of the cumulative number of SGSs during descending phase.
[l] N_{NDSGS}: cumulative number of SGSs in NH during descending phase.
[m] N_{SDSGS}: cumulative number of SGSs in SH during descending phase.
[n] null: no hemisphere is dominant.

unistra.fr/ftp/J/A+A/652/A56/catalb.dat, the comparison of the derived cumulative sunspot numbers and SGSs for the northern and southern hemispheres during the ascending and descending phases of Solar Cycles 17–24 is presented in Table 2. Given the absence of SGSs during the ascending phase of Solar Cycle 17 and throughout Solar Cycle 24, our focus is on comparing the hemispheric asymmetry of cumulative sunspot numbers with that of cumulative SGS numbers originating from the northern and southern hemispheres during the period from the descending phase of Solar Cycle 17 to the end of Solar Cycle 23. As shown in Table 2, the derived cumulative sunspot numbers in the northern and southern hemispheres during the ascending phases of Solar Cycles 18–23 were 16,570 and 14,567, respectively. This indicates that solar activities, as manifested by the cumulative sunspot numbers, were predominantly in the NH during the ascending phases of Solar Cycles 18–23. Consequently, the cumulative number of SGSs with source locations in the NH is larger than that in the SH during the descending phases of Solar Cycles 18–23, consistent with the N–S asymmetry of the cumulative sunspot numbers during these phases.

The derived cumulative sunspot numbers in the northern and southern hemispheres during the descending phases of Solar Cycles 17–23 were 29,258 and 28,573, respectively. This indicates that the cumulative sunspot numbers in the NH were slightly larger than those in the SH during these descending phases. Consequently, solar activity, as indicated by the cumulative sunspot numbers, remained predominantly in the NH during the descending phases of Solar Cycles 17–23. In this context, the cumulative number of SGSs with source locations in the NH is larger than that in the SH during the descending phases of Solar Cycles 18–23, consistent with the N–S asymmetry of the cumulative sunspot numbers during these phases.

During the ascending phases of Solar Cycles 17–23, the difference between the cumulative sunspot numbers in the northern and southern hemispheres was 2003, with a relative difference of 13.8%. In contrast, during the descending phases of Solar Cycles 17–23, the difference was 658, with a relative difference of 2.4%. This clearly shows that the N–S asymmetry, as indicated by the cumulative sunspot numbers, is much stronger during the ascending phases of Solar Cycles 18–23 than during the descending phases of the same cycles 17–23. As shown in Figure 2, the cumulative numbers of the SGSs with source locations in the northern and southern hemispheres during the ascending phases of Solar Cycles 17–23 were 14 and 4, respectively, with a relative difference of 250%. As shown in Figure 3, the cumulative numbers of the SGSs with source locations in the northern and southern hemispheres during the descending phases of Solar Cycles 17–23 were 21 and 12, respectively, with a relative difference of 75%. This indicates that the N–S asymmetry in the cumulative numbers of the SGSs in the two hemispheres is much stronger during the ascending phases of Solar Cycles

18–23 (Figure 2) than during the descending phases of Solar Cycles 17–23 (Figure 3). This is consistent with the asymmetries exhibited by the cumulative sunspot numbers in the two hemispheres during these phases of the same SCs.

From Table 2, it can be seen that during the ascending phase of Solar Cycle 18, the cumulative sunspot number in the NH is lower than that in the SH. However, the cumulative number of SGSs with source locations in the NH is larger than that with source locations in the SH. As shown in Table 2, during the descending phase of Solar Cycle 21, the cumulative number of sunspots in the SH is larger than that in the NH. However, the cumulative number of SGSs with source locations in the NH is larger than that with source locations in the SH. Therefore, during the ascending or descending phases of an SC, a higher cumulative number of sunspots in one hemisphere does not guarantee a higher number of SGSs originating from that hemisphere. In other words, the N–S asymmetry manifested by the cumulative sunspot numbers may differ from the N–S asymmetry manifested by the cumulative SGSs during the ascending phase or descending phase of an SC.

When studying and discussing the N–S asymmetry of solar activity and the differing views among researchers on its origin (e.g., Norton et al. 2014; Hathaway 2015; Deng et al. 2016; Shukuya & Kusano 2017; Schüssler & Cameron 2018; Kitchatinov & Khlystova 2021; Das et al. 2022), CMEs are powerful eruptive events that originate from the Sun. If a CME can lead to a superstorm, then that CME and its driven shock must be able to reach Earth. If a CME and its driven shock do not reach Earth, then this CME event cannot serve as a solar source for an SGS. Therefore, whether a CME can be a solar source of an SGS depends not only on the CME itself but also on whether the CME and its driven shock ultimately reach Earth.

If solar activity (including CMEs) in one hemisphere is stronger than in the other, but fewer superstorm-inducing CMEs from that hemisphere reach Earth compared to the other hemisphere, it can result in a situation where the hemisphere with stronger solar activity produces fewer superstorm-inducing CMEs. Thus, during the ascending or descending phases of a solar activity cycle, it is possible for the hemisphere with stronger solar activity to have fewer superstorm-inducing CMEs than the other hemisphere. However, as shown in Table 2, in most cases, the hemisphere with stronger solar activity also tends to produce more superstorm-inducing CMEs. Thus, the N–S asymmetry of the solar sources of SGSs is essentially in agreement with the N–S asymmetry indicated by sunspot numbers.

Examining the N–S asymmetry of solar activity from the perspective of SCs, the analysis spans Solar Cycles 17–23. During these SCs, the dominant hemisphere for solar activities (including sunspots) was as follows: equal, equal, NH, NH, equal, SH, and SH (Li et al. 2002). Consequently, solar activity across the two hemispheres appears to be largely balanced over the considered timeframe, with two SCs dominated by the NH, two by the SH, and three with equal activity in both hemispheres. However, the solar activities manifested by CMEs that can trigger SGSs during Solar Cycles 17–23 were predominantly in the NH. Therefore, factors beyond solar activity, such as the propagation of the CMEs from the Sun to the Earth, likely contributed to the observed N–S asymmetric distribution of the source locations of SGSs.

It is worth noting that anticorrelation does not inherently imply hemispheric preference. Thus, full anticorrelation can coexist with either symmetry or strong asymmetry. The results in Table 1 already include this meaning.

5. Summary and Conclusion

We investigated the statistical properties of the N–S asymmetry in the source locations of SGSs during different phases of SCs from 1932 to 2018. A total of 54 SGSs were identified during this period, with known source locations for 51 of them. We also analyzed how the N–S asymmetry of the source locations of SGSs evolved with the SC. The key findings are summarized below.

(1) For SGSs that occurred during the ascending phases, the source locations were predominantly in the NH. The N–S asymmetry was significant in the western hemisphere, but not in the eastern hemisphere.

(2) For SGSs that occurred during the descending phases, the NH had a higher number of SGSs compared to the SH. However, the overall N–S asymmetry was not statistically significant. Specifically, significant N–S asymmetry was observed only in the western hemisphere, while no significant asymmetry was detected in the eastern hemisphere.

(3) Between 1932 and 2018, the NH consistently exhibited a greater number of SGSs across varying intensities compared to the SH. The N–S asymmetry was not statistically significant for SGSs with $-300\,\mathrm{nT} < \mathrm{Dst} \leqslant -250\,\mathrm{nT}$ and for those with $\mathrm{Dst} \leqslant -400\,\mathrm{nT}$. However, significant N–S asymmetries were observed for SGSs with $-400\,\mathrm{nT} < \mathrm{Dst} \leqslant -300\,\mathrm{nT}$ and for those with $\mathrm{Dst} \leqslant -300\,\mathrm{nT}$.

(4) We found that, in most cases, the number of SGSs originating in the NH was strongly anticorrelated with the number of SGSs originating in the SH. However, in a few cases, there was no strong inverse correlation between the numbers of SGSs in the northern and southern hemispheres.

(5) From the perspective of the evolution of N–S asymmetry in the source locations of SGSs with the SC, we found that during the ascending phases, the source locations of SGSs consistently dominated in the NH. However, during the descending phases, the source locations of SGSs were predominantly in the NH during Solar Cycles 17–19 and 21, while they were predominantly in the SH during Solar Cycles 20, 22, and 23.

Acknowledgments

We thank the University of Oulu, Finland for providing the Dxt index data and the Center for Geomagnetism and Space

Magnetism, Kyoto University, for providing the Dst index data. We also thank the WDC-SILSO, Royal Observatory of Belgium in Brussels, for providing the smoothed monthly mean sunspot numbers (SMMSNs), and Veronig et al. (2021) for providing the monthly sunspot numbers for the northern and southern hemispheres.

Dcx can be accessed via http://dcx.oulu.fi. The smoothed monthly mean sunspot numbers can be obtained from the website at http://sidc.oma.be/silso/datafiles. The monthly sunspot numbers for the northern and southern hemispheres are available from the website at https://cdsarc.cds.unistra.fr/ftp/J/A+A/652/A56/catalb.dat.

This work was supported by the National Natural Science Foundation of China (NSFC, grant Nos. 41774085, 41074132, 41274193 and 41674166) and the Special Fund of the Institute of Geophysics, China Earthquake Administration (grant Nos. DQJB22X12 and DQJB24X25).

Appendix
List of SGSs During 1932–2018

The time information including year, month and day, the Dst index, the source location and SC information for each SGS are listed in Table A1.

Table A1
The Time and Source Locations' Information of the SGSs

No.	SC	Amplitude	Year	Month	Day	Dst (nT)	Location	Reference
1	17	198.6	1938	1	22	−340	N17W30	Cliver2022*
2	⋯	⋯	1938	1	25	−350	N15W69	Cliver2022
3	⋯	⋯	1938	4	16	−256	N23W11	Lefèvre2016*
4	⋯	⋯	1939	4	25	−250	N28E59	Lefèvre2016
5	⋯	⋯	1940	3	24	−356	N12E37	Cliver2022
6	⋯	⋯	1940	3	30	−266	unknown	⋯
7	⋯	⋯	1941	3	1	−456	N14W13	Cliver2022
8	⋯	⋯	1941	7	5	−451	N14E04	Cliver2022
9	⋯	⋯	1941	9	19	−415	N11W09	Cliver2022
10	18	218.7	1946	3	28	−481	N20E05	Cliver2022
11	⋯	⋯	1946	7	27	−268	N20E15	Lefèvre2016
12	⋯	⋯	1949	1	25	−309	N23E01	Cliver2022*
13	⋯	⋯	1949	5	12	−258	S20E12	Lefèvre2016
14	⋯	⋯	1950	8	20	−278	unknown	⋯
15	19	285.0	1956	4	27	−259	unknown	⋯
16	⋯	⋯	1957	1	22	−250	S30W18	Meng2019*
17	⋯	⋯	1957	3	2	−255	N18W35	Meng2019
18	⋯	⋯	1957	9	5	−324	N23W30	Cliver2022
19	⋯	⋯	1957	9	13	−427	N13W02	Cliver2022
20	⋯	⋯	1957	9	23	−303	N10W06	Cliver2022
21	⋯	⋯	1958	2	11	−426	S12W14	Cliver2022
22	⋯	⋯	1958	7	8	−330	N25W08	Cliver2022
23	⋯	⋯	1958	9	4	−302	S08E84	Cliver2022
24	⋯	⋯	1960	7	15	−429	N17E04	Cliver2022
25	⋯	⋯	1960	4	1	−327	N12E11	Cliver2022
26	⋯	⋯	1960	4	30	−325	N10W22	Cliver2022
27	⋯	⋯	1960	10	7	−287	S18E41	Lefèvre2016
28	⋯	⋯	1960	11	13	−339	N28E12	Cliver1993
29	⋯	⋯	1961	10	28	−272	N27W08	Cliver1993
30	20	156.6	1967	5	26	−387	N28E26	Cliver2022
31	⋯	⋯	1970	3	8	−284	S11E09	Meng2019
32	21	232.9	1981	4	13	−311	N06W06	Cliver2022
33	⋯	⋯	1982	7	14	−325	N11E36	Cliver2002
34	⋯	⋯	1982	9	6	−289	N10E36	Meng2019
35	⋯	⋯	1986	2	9	−307	S11W21	Cliver2022
36	22	212.5	1989	3	14	−589	N32E22	Cliver2022
37	⋯	⋯	1989	9	19	−255	N20W24	Cliver1993
38	⋯	⋯	1989	10	21	−268	S27E10	Meng2019
39	⋯	⋯	1989	11	17	−266	N11W26	Meng2019
40	⋯	⋯	1990	4	10	−281	N24E29	Meng2019
41	⋯	⋯	1991	3	25	−298	S26E28	Meng2019
42	⋯	⋯	1991	10	29	−254	S13E15	Meng2019

Table A1
(Continued)

No.	SC	Amplitude	Year	Month	Day	Dst (nT)	Location	Reference
43	⋯	⋯	1991	11	9	−354	S35E22	Cliver2022
44	⋯	⋯	1992	5	10	−288	S26E08	Meng2019
45	23	180.3	2000	4	7	−288	N15W66	Meng2019
46	⋯	⋯	2000	7	16	−301	N22W07	Cliver2022
47	⋯	⋯	2001	3	31	−387	N16W12	Cliver2022
48	⋯	⋯	2001	4	11	−271	S23W09	Meng2019
49	⋯	⋯	2001	11	6	−292	N06W18	Meng2019
50	⋯	⋯	2003	10	30	−353	S16E08	Cliver2022
51	⋯	⋯	2003	10	30	−383	S15W02	Cliver2022
52	⋯	⋯	2003	11	20	−422	S20E20	Cliver2022
53	⋯	⋯	2004	11	8	−374	N10E08	Cliver2022
54	⋯	⋯	2004	11	10	−263	N09W17	Meng2019

Note. Cliver2022* (Cliver et al. 2022), Lefèvre2016* (Lefèvre et al. 2016), Meng2019* (Meng et al. 2019).

ORCID iDs

Qi Li https://orcid.org/0009-0005-5721-2906
Gui-Ming Le https://orcid.org/0000-0002-9906-5132

References

Ataç, T., & Özgüç, A. 1996, SoPh, 166, 201
Badalyan, O. G., & Obridko, V. N. 2011, NewA, 16, 357
Carbonell, M., Oliver, R., & Ballester, J. L. 1993, A&A, 274, 497
Carbonell, M., Terradas, J., Oliver, R., & Ballester, J. L. 2007, A&A, 476, 951
Chapman, S. C., & Dudok de Wit, T. 2024, NatSR, 14, 8249
Chapman, S. C., McIntosh, S. W., Leamon, R. J., & Watkins, N. W. 2020, GeoRL, 47, e87795
Cliver, E. W., & Crooker, N. U. 1993, SoPh, 145, 347
Cliver, E. W., Potzi, W., & Veronig, A. M. 2022, ApJ, 938, 136
Das, R., Ghosh, A., & Karak, B. B. 2022, MNRAS, 511, 472
Deng, L., Zhang, X., An, J., & Cai, Y. 2017, JSWSC, 7, A34
Deng, L. H., Xiang, Y. Y., Qu, Z. N., & An, B. B. 2016, AJ, 151, 70
Dubyagin, S., Ganushkina, N., Kubyshkina, M., & Liemohn, M. 2014, JGRA, 119, 7243
Ganushkina, N., Jaynes, A., & Liemohn, M. 2017, SSRv, 212, 1315
Ganushkina, N. Y., Liemohn, M. W., Dubyagin, S., et al. 2015, AnGeo, 33, 1369
Garcia, H. A., & Dryer, M. 1987, SoPh, 109, 119
Gopalswamy, N., Yashiro, S., Akiyama, S., et al. 2022, JGRA, 127, e2022JA030404
Gopalswamy, N., Yashiro, S., Liu, Y., et al. 2005a, JGRA, 109, S15
Gopalswamy, N., Yashiro, S., Michalek, G., Xie, H., et al. 2005b, GeoRL, 32, L12S09
Gosling, J. T., McComas, D. J., Phillips, J. L., et al. 1991, JGR, 96, 7831
Hajra, R., Tsurutani, B. T., Echer, E., Gonzalez, W. D., & Gjerloev, J. W. 2016, JGRD, 121, 7805
Hathaway, D. H. 2015, LRSP, 12, 4
Huttunen, K. E. J., Koskinen, H. E. J., & Schwenn, R. 2002a, JGRA, 107, 1121
Huttunen, K. E. J., Koskinen, H. E. J., Pulkkinen, T. I., et al. 2002b, JGRA, 107, 1440
Joshi, B., & Joshi, A. 2004, SoPh, 219, 343
Karinen, A., & Mursula, K. 2005, AnGeo, 23, 475
Kilpua, E. K. J., Olspert, N., Grigorievskiy, A., et al. 2015, ApJ, 806, 272
Kitchatinov, L., & Khlystova, A. 2021, ApJ, 919, 36
Knaack, R., Stenflo, J. O., & Berdyugina, S. V. 2004, A&A, 418, L17
Lakhina, G. S., Alex, S., Tsurutani, B. T., & Gonzalez, W. D. 2012, in Extreme Events and Natural Hazards: The Complexity Perspective, ed. A. S. Sharma et al. (Washington, D.C.: American Geophysical Union), 267
Larson, H. J. 1982, Introduction to Probability Theory and Statistical Inference, 3rd ed. (New York: Wiley, Inc)
Le, G. M., & Liu, G. A. 2020, SoPh, 295, 35
Le, G. M., Liu, G. A., Zhao, M. X., Mao, T., & Xu, P. G. 2021a, RAA, 21, 130
Le, G. M., Zhang, Y. N., & Zhao, M. X. 2021b, SoPh, 296, 16
Le, G. M., Zhao, M. X., Li, Q., et al. 2021c, MNRAS, 502, 2043
Le, G. M., Zhao, M. X., Zhang, W. T., & Liu, G. A. 2021d, SoPh, 296, 187
Li, K. J., & Gu, X. M. 2000, A&A, 353, 396
Lefèvre, L., Vennerstrøm, S., Dumbović, M., et al. 2016, SoPh, 291, 1483
Li, K.-J., Wang, J.-X., Xiong, S.-Y., et al. 2002, A&A, 383, 648
Li, K. J., Yun, H. S., & Gu, X. M. 2001, ApJ, 554, L115
Li, Q., & Le, G.-M. 2025, SoPh, 300, 101
Love, J. J. 2021, SpWea, 19, e02579
Maltsev, Y. 2004, SSRv, 110, 227
Meng, X., Tsurutani, B. T., & Mannucci, A. J. 2019, JGRA, 124, 3926
Norton, A. A., Charbonneau, P., & Passos, D. 2014, SSRv, 186, 251
Owens, M. J., Lockwood, M., Barnard, L. A., et al. 2021, SoPh, 296, 82
Pick, L. J. L., & Korte, M. 2017, GeoJI, 211, 1223
Richardson, I. G., & Cane, H. V. 2012, JSWSC, 2, A01
Riley, P. 2018, in Extreme Events in Geospace, ed. N. Buzulukova (Amsterdam: Elsevier), 115
Schüssler, M., & Cameron, R. H. 2018, A&A, 618, A89
Shukuya, D., & Kusano, K. 2017, ApJ, 835, 84
Srivastava, N. 2005, AnGeo, 23, 2989
Takalo, J. 2021, SoPh, 296, 19
Temmer, M., Rybýk, J., Bendík, P., et al. 2006, A&A, 447, 735
Venkatakrishnan, P., & Ravindra, B. 2003, GeoRL, 30, 2181
Vennerstrom, S., Lefevre, L., Dumbović, M., et al. 2016, SoPh, 291, 1447
Verma, V. K. 1993, ApJ, 403, 797
Veronig, A. M., Jain, S., Podladchikova, T., Pötzi, W., & Clette, F. 2021, A&A, 652, A56
Wang, Y. M., Ye, P. Z., & Wang, S. 2003, JGRA, 108, 1370
Yakovchouk, O. S., Mursula, K., Holappa, L., et al. 2012, JGRA, 117, A03201
Yermolaev, Y., Zelenyi, L. M., Kuznetsov, V. D., et al. 2008, JASTP, 70, 334
Yermolaev, Y. I., Lodkina, I. G., Nikolaeva, N. S., et al. 2013, JGRA, 118, 4760
Zhang, J., Richardson, I. G., Webb, D. F., et al. 2007, JGRA, 112, A10102
Zhang, X., Deng, L., et al. 2024, ApJ, 962, 172
Zhang, X. J., Deng, L. H., Fei, Y., et al. 2022, MNRAS, 514, 1140
Zhao, M.-X., Le, G.-M., & Liu, Y.-H. 2022, Univ, 8, 605
Zhao, M.-X., Le, G.-M., & Liu, Y.-H. 2023, RAA, 23, 015007